Design of Wideband Omnidirectional Dual-Reflector Antennas in Millimeter Waves

Rafael A. Penchel, Sandro R. Zang, José R. Bergmann, *Member, IEEE*, and Fernando J. S. Moreira, *Senior Member, IEEE*

***Abstract*—The work investigates the electromagnetic performance of omnidirectional dual-reflector antennas designed to operate with a frequency bandwidth larger than 45% (25–40 GHz). We consider two antenna configurations, distinguished from each other by two different optical ray mappings. A conventional coaxial horn is designed to ensure vertical polarization and stable primary radiation pattern along the operating bandwidth. By employing a geometrical optics synthesis technique, the omnidirectional reflectors are shaped to maximize the directivity of the broadside secondary radiation patterns. For the synthesis, we employ different aperture power distributions and investigate their effect on the antenna gain and return loss when operating over the 40% frequency bandwidth. To access the antenna performance, a full-wave electromagnetic analysis based on the combination of mode matching and method of moments is employed.**

***Index Terms*—Omnidirectional antennas, reflector antennas, ultra-wideband antennas.**

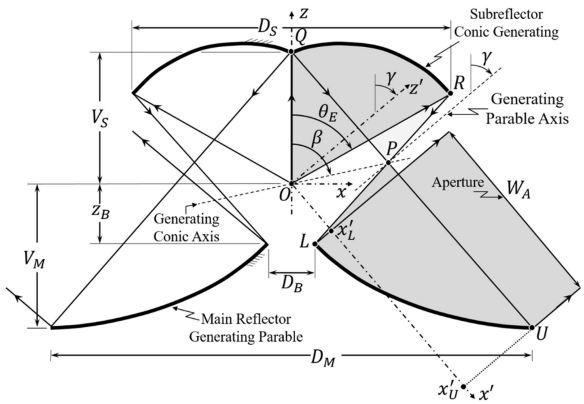

Fig. 1. Omnidirectional dual-reflector antenna design parameters.

I. Introduction

LARGE data rates required by new communication services have inspired the development of systems operating at higher frequencies, e.g., millimeter-wave band [1]. At these frequencies, highly efficient shaped single and dual reflectors have been investigated for omnidirectional coverages [2] and [9]. As extensively discussed in [2] and [6], the dual cases lead to more compact designs than the single cases, as the dual configurations require a considerably smaller reflector diameter to achieve the same aperture field distribution. Synthesis techniques based on geometrical optics (GO) have been employed to explore omnidirectional dual-reflector antennas shaped to offer a prescribed radiation pattern in the elevation plane [2]–[7]. For a specific design frequency, successful examples have been synthesized [2]–[7]. Some works have dealt with designs suited to provide cosecant squared radiation patterns in the elevation plane to attain base stations with uniform area coverages, but with frequency bandwidths less than 10%, e.g., at 27.5–29.5 GHz in [8] and 40.5–42.5 GHz in [9], both with return losses above 20 dB.

For large operating bandwidths, the effectiveness of the GO shaping techniques relies on the stability of the feed primary radiation pattern across the band to ensure the control of the antenna radiation pattern [10]. Additionally, geometry compactness may affect the feed return loss due to interactions between feed and, particularly, subreflector. Reflector shaping may even increase such interactions, imposing further limitations on the antenna electromagnetic performance.

The present study explores the electromagnetic performance—secondary radiation pattern and return loss—of highly efficient omnidirectional dual-reflector antennas (see Fig. 1) designed to operate across a 40% bandwidth (25–40 GHz). Two antenna configurations are considered, which are distinguished from each other by different optical ray mappings (from the primary focus to the dual-reflector conical aperture), similarly to the discussion in [6]. The reflectors' generatrices are shaped to maximize the directivity of the secondary pattern by redistributing the feed energy over the antenna (conical) aperture while diminishing scattering toward the horn's aperture to sustain the desired return-loss level across the operating band. To ensure vertical polarization, a coaxial horn feeds the circular symmetric reflector antennas [3]–[7]. Here, we compare the performance of antennas synthesized to attend two different aperture power distributions to investigate the tradeoff between directivity and return loss. To estimate the electromagnetic performance, a rigorous full-wave analysis combining mode matching technique (MMT), to calculate the fields inside the feed structure, and method of moments (MoM), to calculate the fields outside the feed horn, is employed. Such analysis not only accurately

Manuscript received February 7, 2019; accepted March 12, 2019. Date of publication March 18, 2019; date of current version May 3, 2019. This work was supported in part by the CNPq, FAPEMIG, and CAPES-PROCAD under Grant 068419/2014-01. *(Corresponding author: José R. Bergmann.)*

R. A. Penchel is with the São Paulo State University (UNESP), São João da Boa Vista, SP 13876-750, Brazil (e-mail: rafael.penchel@unesp.b).

S. R. Zang is with the Federal University of São João Del Rei, Ouro Branco, MG 36.420-000, Brazil (e-mail: szang@ufsj.edu.br).

J. R. Bergmann is with the Pontifical Catholic University of Rio de Janeiro, Rio de Janeiro, RJ 22453-900, Brazil (e-mail: bergmann@puc-rio.br).

F. J. S. Moreira is with the Federal University of Minas Gerais, Belo Horizonte, MG 31270-901, Brazil (e-mail: fernandomoreira@ufmg.br).

Digital Object Identifier 10.1109/LAWP.2019.2905602

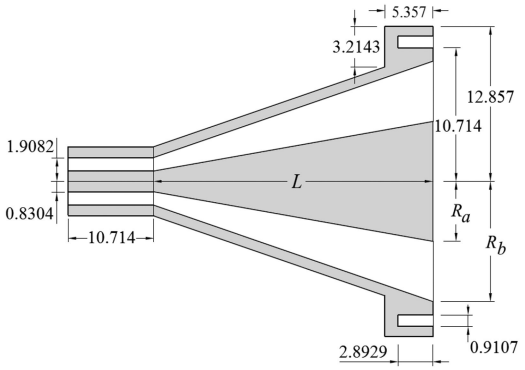

Fig. 2. Coaxial horn dimensions in millimeters.

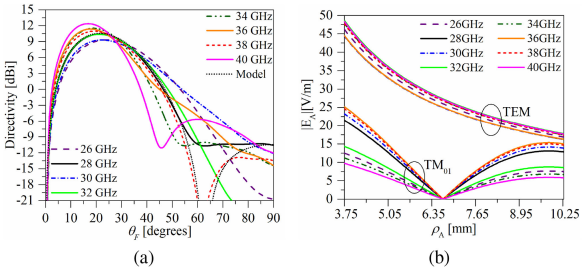

Fig. 3. Coaxial horn MMT/MoM (a) radiation patterns and GO feed model and (b) mode amplitude at horn's aperture.

estimates the antenna secondary radiation pattern but also the return loss associated with the modes reflected back into the feed waveguide [11], [12]. The results provided by MoM/MMT were successfully validated against those yielded by the CST Studio Suite, as shown in [11] and [12]. This work is organized as follows. Section II shows the design of the coaxial horn. Section III presents the numerical analysis of the antennas' secondary radiation patterns for the several configurations investigated here. Conclusions are presented in Section IV.

II. Coaxial Feed Horn

To ensure dual-reflector antennas with vertical polarization, a conventional coaxial horn was employed as feeder, and its geometry suited to provide a stable primary radiation pattern to illuminate the reflector antennas across the operating bandwidth. Fig. 2 shows the horn designed to operate between 25 and 40 GHz. By embedding the MoM/MMT analysis in an optimization scheme, the dimensions L, R_a, and R_b were optimized to reduce the variation of the radiation pattern at $0^\circ \leq \theta_F \leq 55^\circ$ across the bandwidth [see Fig. 3(a)] while providing a return loss above 20 dB. Although it was not the focus of the present study, the optimization of the feed chain may lead to further reduction of return loss. A choke was introduced at the aperture plane (Fig. 2) to reduce induced currents on the horn's external surface.

At the band's lower frequencies, the transverse electromagnetic (TEM) mode dominates the horn aperture modal distribution, generating a radiation pattern with a main lobe that is continuously narrowed as frequency increases, leading to a poor illumination of the dual-reflector system and reducing radiation efficiency. To compensate this deleterious frequency dependency, dimensions $L = 23.25$ mm, $R_a = 3.75$ mm, and $R_b = 10.28$ mm were optimized to control return loss while allowing the presence of high-order mode (TM_{01}) at the horn's aperture for higher frequencies where $R_b - R_a > \lambda/2$. The mode TM_{10} radiates at wide θ_F angles, compensating the narrowing of the horn's radiation pattern and, consequently, reducing its frequency dependence. To illustrate this behavior, Fig. 3(a) shows the horn's radiation patterns from 25 to 40 GHz provided by the MMT/MoM technique. The horn aperture field expansion provided by the TEM and TM_{0n} modes couples both numerical techniques, and the solution yields the coefficients of the expansion [11]. Fig. 3(b) compares the amplitude distribution of the modes TEM and TM_{01} at the horn's aperture for sample frequencies. As observed from these figures, the shape of the main lobe is affected by amplitude of the TM_{01} excited at the horn's aperture, widening as the TM_{01} amplitude increases. However, the presence of the higher mode can bring phase variation at the antenna aperture.

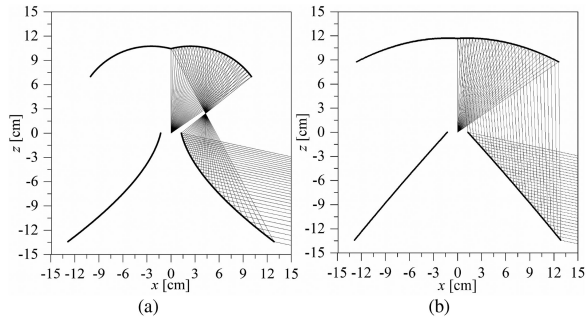

Fig. 4. Generatrices and rays tracing of the classical (a) OADE and (b) OADC cases.

III. Dual-Reflector Antenna Wideband Performance

To explore the wideband behavior of omnidirectional dual-reflector antennas, two configurations are investigated: one based on the axially displaced Cassegrain (OADC) geometry and the other on the axially displaced ellipse (OADE) configuration, which is illustrated in Fig. 1. Their main characteristics and features are fully discussed in [4]–[7]. Initially, classical geometries (i.e., with their body-of-revolution reflectors generated by conic sections) are considered [4], [5]. Afterwards, their reflectors are shaped to maximize the overall antenna gain across the operating band without changing the feed horn. The GO shaping technique adopted here, is that of [12].

A. Classical Omnidirectional Dual-Reflector Antennas

The design procedure of classical omnidirectional dual-reflector antennas is extensively discussed in [4] and [5]. The notation of [5] is adopted here, and the principal parameters are illustrated in Fig. 1. Both OADE and OADC configurations were designed to have maximum radiation at $\theta = \gamma = 102^\circ$ in the vertical plane, main reflector aperture width $W_A = 107.14$ mm (i.e., approximately 10λ at 28 GHz), main reflector diameter $D_M = 237.14$ mm, central-opening diameter $D_B = 25.71$ mm, and primary focus O at the main reflector central-opening plane ($z_B = 0$). The parameter V_S was adjusted to have $\theta_E \approx 55^\circ$ for both configurations. Fig. 4(a) and (b) shows the OADE and OADC reflector generatrices, respectively, together with optical rays. Table I lists the parameters of the subreflector's generatrices [5].

TABLE I
SUBREFLECTOR PARAMETERS OF THE CLASSICAL ANTENNAS

Parameteres	OADE	OADC
Eccentricity e	0.253444	0.833930
Tilt Angle β	60.68°	173.09°
Interfocal Distance 2c (mm)	49.56	1169.02
Diameter D_B (mm)	200.75	251.93
Feed Distance V_S (mm)	104.46	116.79

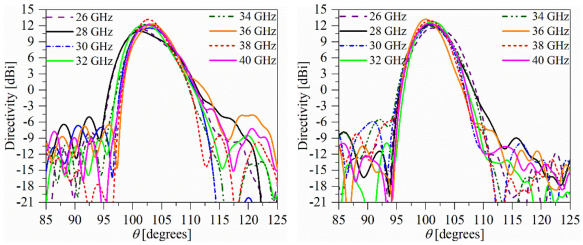

(a) (b)

Fig. 5. Radiation patterns of classical (a) OADE and (b) OADC cases.

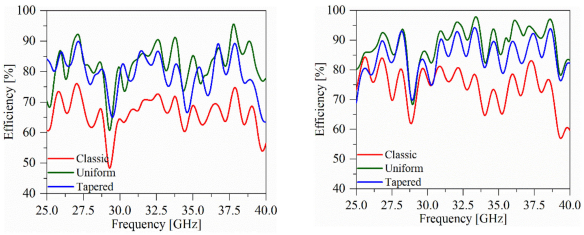

(a) (b)

Fig. 6. Antenna efficiency of the (a) OADE and (b) OADC cases.

Fig. 5(a) and (b) shows the radiation patterns of the OADE and OADC antennas, respectively, obtained from the MMT/MoM analysis technique. There, it is possible to observe a small mainlobe shoulder, indicating small non-uniformities in the phase distribution over the main reflector aperture at lower frequencies. Fig. 6(a) and (b) shows the efficiency for both configurations, by comparing with the maximum possible directivity D_{MAX}, according to [5, Eq. (24)]. As observed, the OADC antenna shows higher efficiencies when compared with the OADE antenna. For both cases, the efficiency shows ripples due to the interaction between reflectors and feed.

B. Configurations Shaped for Maximum Efficiency

To evaluate the effects of the reflectors' shaping on the antenna performance, first, the GO synthesis technique of [12] was applied to shape main and subreflectors, imposing uniform phase and power distributions over the main reflector conical aperture to maximize directivity. For the GO synthesis, the coaxial horn radiation was modeled as a spherical wavefront with circularly symmetric radiation pattern $G_F(\theta_F)$ [6]:

$$G_F(\theta_F) = G_{F0}\left[\frac{J_0(ka_i \sin\theta_F) - J_0(ka_e \sin\theta_F)}{\sin\theta_F}\right]^2 \quad (1)$$

for $\theta_F \leq \pi/2$, with phase center at O (Fig. 1). In (1), $J_0(\cdot)$ is the Bessel function of order zero, G_{F0} is a normalization factor, $k = 2\pi/\lambda$, and the equivalent radii of the horn's aperture $a_i = 3.86$ mm and $a_e = 12.0$ mm were adjusted to match the MMT/MoM feed radiation pattern at 28 GHz, as shown in Fig. 3.

TABLE II
GEOMETRIC PARAMETERS OF THE SHAPED ANTENNAS IN MILLIMETERS

Antenna	W_A	D_M	V_M	D_S	V_S	D_B	z_B
OADE	107.14	257.14	132.90	208.61	104.46	37.27	− 1.23
OADC	107.14	251.35	133.52	249.50	116.79	25.714	0

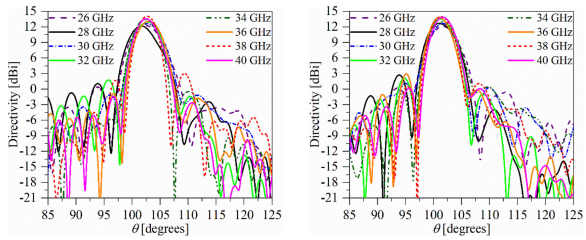

(a) (b)

Fig. 7. Radiation patterns of (a) OADE and (b) OADC uniform cases.

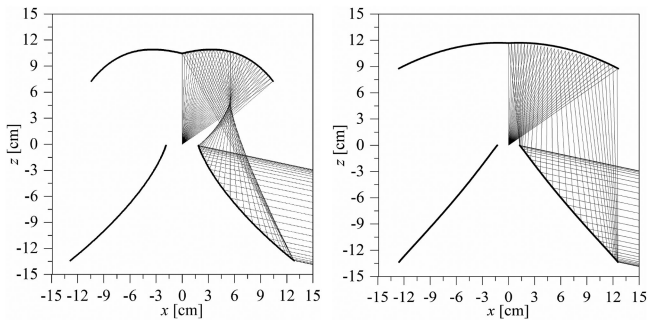

(a) (b)

Fig. 8. Generatrices and rays tracing of (a) OADE and (b) OADC uniform cases.

For comparative purposes, W_A and V_S still have the same values adopted for the classical configurations, and the remaining parameters obtained from the GO synthesis are listed in Table II. Fig. 7(a) and (b) shows the shaped reflectors' generatrices and the optical rays, where one observes the concentration of rays at both edges of the main reflector conical aperture to compensate for the lower feed illumination toward the subreflector's center and rim (see Fig. 3).

Fig. 7(a) and (b) shows the radiation patterns of the OADE and OADC antennas shaped for uniform aperture phase and power distribution, respectively, for several frequencies between 26 and 40 GHz. The antenna efficiencies shown in Fig. 6(a) and (b) clearly indicate the success of the reflectors' shaping in maximizing the antenna directivity, as desired. However, the concentration of rays around the horn's aperture brought by the reflectors' shaping (see Fig. 8) compromises the return loss performance. To illustrate this effect, Fig. 9(a) and (b) depicts the antenna return loss calculated by the MMT/MoM technique at 26–40 GHz for the OADE and OADC antennas. As reference, the return loss of the horn alone is also included (black line). From Fig. 10(a), one observes that the mutual coupling among horn and reflectors is crucial, imposing return-loss increases of

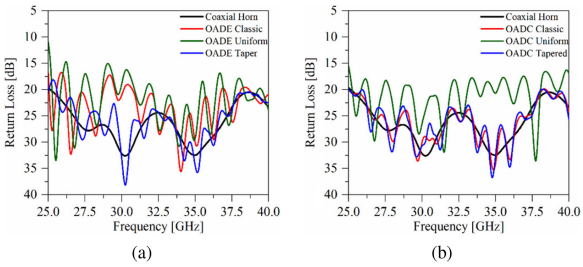

Fig. 9. Antenna return loss of the (a) OADE and (b) OADC cases.

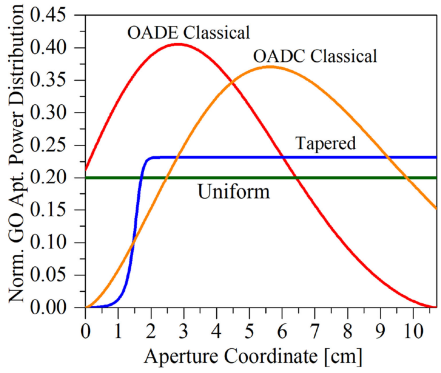

Fig. 10. GO aperture power distribution.

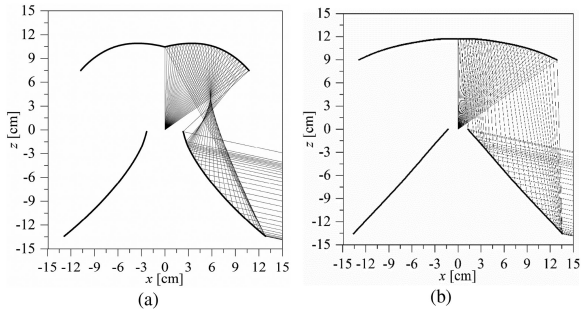

Fig. 11. Generatrices and rays tracing of the (a) OADE and (b) OADC tapered cases.

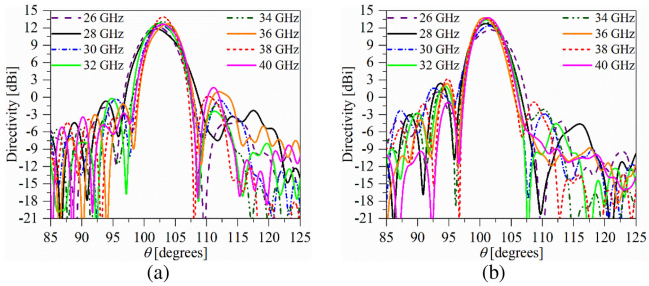

Fig. 12. Radiation patterns of (a) OADE and (b) OADC tapered cases.

5 dB or higher across the band for both classical and shaped-uniform OADE. The return loss is more intense at lower frequencies and rises again at 30 GHz, when the primary feed radiation mainlobe is wider (Fig. 3), thus raising the subreflector's edge illumination. At higher frequencies, the return loss diminishes as the feed mainlobe is narrowed down. From Fig. 10(b), one observes that the shaped uniform OADC has a similar behavior. Among all antennas investigated so far, the only one where mutual coupling does not significantly affect return loss is the classical OADC, for which scattering toward the horn's aperture is relatively small.

C. Configurations Shaped to Reduce Return Loss

An alternative design that increases the antenna directivity without significantly compromising the feed return loss may be obtained by using a tapering on the power distribution at the main reflector conical aperture during the GO synthesis. The following power distribution was chosen [12]:

$$G(x') = \begin{cases} G_0\left\{\left[\frac{2(x\prime - x'_o)}{\sigma_1 W_A}\right]^{\sigma_2} + 1\right\}^{-2\sigma_3}, & \text{for } x'_L \le x\prime \le x'_o \\ G_0, & \text{for } x'_o \le x\prime \le x'_U \end{cases} \quad (2)$$

where G_0 is a normalization factor and A, σ_2, and σ_3 are adjusted to attain the desired antenna performance. Fig. 10 depicts the power distribution given by (2), comparing it with the uniform distribution previously adopted, those provided by the classical configurations, and that given by (2) for $\sigma_1 = 0.70$, $\sigma_2 = 40.0$, and $\sigma_3 = 0.242$, with x'_o at the center of the aperture. As observed, the tapered distribution combines an almost uniform distribution in most of the aperture with fast decay around the aperture extreme at x'_L, reducing the subreflector scattering toward the horn's aperture (see Fig. 1 for the OADE).

Fig. 11(a) and (b) shows the shaped generatrices and the ray tracing resulting from the synthesis; Fig. 12(a) and (b) shows the MoM/MMT antenna radiation pattern at the sampling frequencies. As observed in ray tracing, the shaping concentrates the rays at the bottom edge, similar to the uniform case, disperses them at the top of the aperture lowering the top edge illumination, and decreases the energy reradiated towards the feed horn opening. The effects can be observed in Fig. 6(a) and (b) where the return loss has been reduced, especially for OADE case without significant decrease in the antenna gain.

IV. Conclusion

To operate in millimeter-wave frequencies, the design performance of omnidirectional dual-reflector antennas suited was explored. Two compact configurations, an OADE type and an OADC type, were designed to attain a main beam direction at $\theta = 102^\circ$ with respect to the symmetry axis and simultaneously control the antennas return loss. GO synthesis technique was employed to shape the reflectors, and a hybrid technique based on MoM/MMT was used to analyze the compact antenna designs. Although the compact design increases the coupling between feed and reflectors, and brings some fluctuations in the efficiency along the wide band, the reflector shaping was very effective to maximize the antenna gain and to control the antenna return loss over a frequency band larger than 45% (25–40 GHz).

REFERENCES

[1] T. S. Rappaport, R. W. Heath Jr., R. C. Daniels, and J. N. Murdock, *Millimeter Wave Wireless Communications*. Englewood Cliffs, NJ, USA: Prentice Hall, 2015.

[2] A. P. Norris and W. D. Waddoup, "A millimetric wave omnidirectional antenna with prescribed elevation shaping," in *Proc. ICAP – 4th Int. Conf. Antennas Propag.*, 1985, pp. 141–145.

[3] A. G. Pino, A. M. A. Acuña, and J. O. R. Lopez, "An omnidirectional dual-shaped reflector antenna," *Microw. Opt. Technol. Lett.*, vol. 27, no. 5, pp. 371–374, Dec. 2000.

[4] F. J. S. Moreira and J. R. Bergmann, "Classical axis-displaced dual-reflector antennas for omnidirectional coverage," *IEEE Trans. Antennas Propag.*, vol. 53, no. 9, pp. 2799–2808, Sep. 2005.

[5] F. J. S. Moreira and J. R. Bergmann, "Axis-displaced dual-reflector antennas for omnidirectional coverage with arbitrary main-beam direction in the elevation plane," *IEEE Trans. Antennas Propag.*, vol. 54, no. 10, pp. 2854–2861, Oct. 2006.

[6] F. J. S. Moreira, A. Prata Jr., and J. R. Bergmann, "GO shaping of omnidirectional dual-reflector antennas for a prescribed equi-phase aperture field distribution," *IEEE Trans. Antennas Propag.*, vol. 55, no. 1, pp. 99–106, Jan. 2007.

[7] J. R. Bergmann and F. J. S. Moreira, "Omnidirectional ADE antenna with GO shaped main reflector for arbitrary far-field pattern in the elevation plane," *Microw., Antennas Propag.*, vol. 3, no. 5, pp. 1028–1035, Oct. 2009.

[8] P. Besso, R. Bills, P. Brachat, and R. Vallauri, "A millimetric wave omnidirectional antenna with cosecant squared elevation pattern," in *Proc. ICAP 10th Int. Conf. Antennas Propag.*, vol. 1, 1997, pp. 448–451.

[9] R. Vallauri, P. Besso, A. Avitabile, R. Bills, and R. Brachat, "Azimuthally omnidirectional antenna with vertical or horizontal polarisation for LMDS in the 40 GHz Band," in *Proc. Millennium Conf. Antennas Propag. (AP2000)*, D. Danesy and H. Sawaya, Eds., Davos, Switzerland, 2000, p. 555.

[10] J. R. Bergmann and F. J. S. Moreira, "Bandwidth behavior of omnidirectional dual-reflector antennas synthesized for uniform coverage," *J. Microw. Optoelectron. Electromagn. Appl.*, vol. 8, no. 1, pp. S1–S8, Jun. 2009.

[11] S. R. Zang and J. R. Bergmann, "Analysis of omnidirectional dual-reflector antenna and feeding horn using moment methods," *IEEE Trans. Antennas Propag.*, vol. 62, no. 3, pp. 1534–1538, Mar. 2014.

[12] R. A. Penchel, S. R. Zang, J. R. Bergmann, and F. J. S. Moreira, "GO shaping of omnidirectional dual-reflector antennas with arbitrary main-beam direction in elevation plane by connecting conic sections," *Int. J. Antennas Propag.*, vol. 2018, 2018, Art. no. 1409716.